Gold as Hydrogen. An Experimental and Theoretical Study of the Structures and Bonding in Disilicon Gold Clusters $Si_2Au_n^-$ and Si_2Au_n ($n = 2$ and 4) and Comparisons to Si_2H_2 and Si_2H_4

Xi Li, Boggavarapu Kiran, and Lai-Sheng Wang*

Department of Physics, Washington State University, 2710 University Drive, Richland, Washington 99352, and W. R. Wiley Environmental Molecular Sciences Laboratory and Chemical Sciences Division, Pacific Northwest National Laboratory, P.O. Box 999, MS K8-88, Richland, Washington 99352

Received: March 10, 2005

In a previous communication, we showed that a single Au atom behaves like H in its bonding to Si in a series of Si−Au clusters, $SiAu_n$ ($n = 2-4$) (Kiran et al. *Angew. Chem., Int. Ed*. **2004**, *43*, 2125). In this article, we show that the H analogy of Au is more general. We find that the chemical bonding and potential energy surfaces of two disilicon Au clusters, Si_2Au_2 and Si_2Au_4, are analogous to Si_2H_2 and Si_2H_4, respectively. Photoelectron spectroscopy and ab initio calculations are used to investigate the geometrical and electronic structures of $Si_2Au_2^-$, $Si_2Au_4^-$, and their neutral species. The most stable structures for both Si_2Au_2 and $Si_2Au_2^-$ are found to be C_{2v}, in which each Au bridges the two Si atoms. For $Si_2Au_4^-$, two nearly degenerate dibridged structures in a cis (C_{2h}) and a trans (C_{2v}) configuration are found to be the most stable isomers. However, in the neural potential energy surface of Si_2Au_4, a monobridged isomer is the global minimum. The ground-state structures of $Si_2Au_2^-$ and $Si_2Au_4^-$ are confirmed by comparing the computed vertical detachment energies with the experimental data. The various stable isomers found for Si_2Au_2 and Si_2Au_4 are similar to those known for Si_2H_2 and Si_2H_4, respectively. Geometrical and electronic structure comparisons with the corresponding silicon hydrides are made to further establish the isolobal analogy between a gold atom and a hydrogen atom.

Introduction

Gold is a unique element and possesses chemistry very different from the lighter coinage metals. It is now well recognized that the unusual gold chemistry can be explained by the relativistic effects.[1] At a fundamental level, these effects stabilize the 6s orbital and destabilize the 5d orbitals of gold.[2] As a result, gold has an anomalously high electron affinity (comparable to that of iodine) and readily forms alkali−Au compounds, in which Au is the electron acceptor (Au^{1-}).[3] Indeed analogies between gold and the halogens have been observed and novel halide-like molecules of Au have been proposed.[3c] Due to the decreased energy gap between the 6s and 5d orbitals, their tendency to hybridize (s−d hybridization) is quite high, resulting in the existence of a wide range of oxidation states for Au compared to Cu or Ag. However, the most remarkable chemistry of gold is the isolobal analogy between a gold phosphine unit ($AuPR_3$) and hydrogen.[4] Lauher and Wald were among the first to notice the structural similarity between transition-metal hydrides and the corresponding $Au-PPh_3$ derivatives ($Ph = C_6H_5$).[4b] For example, both $H-FeCo_3(CO)_{12}$ and $FeCo_3(CO)_{12}-AuPPh_3$ adopt trigonal-bipyramidal geometries in which one of the apex atom positions is occupied by H or $AuPPh_3$. Mingos provided theoretical justifications for the $H/AuPR_3$ analogy using the extended Huckel theory.[4a,c] In the trisgold oxonium $[O(AuPPh_3)_3]^+$ and tetragold ammonium $[N(AuPPh_3)_4]^+$ ions the $[AuPPh_3]^+$ unit has been considered as an analogue to a proton (H^+).[5] However, the most dramatic application of this analogy was the synthesis of hypercoordinate compounds, such as octahedral $C(AuPPh_3)_6^{2+}$ and pentagonal-bipyramidal $C(AuPPh_3)_5^+$ cations.[6] Further stabilized by the aurophilic interactions, these polyaurated cations made it possible to study the nature of hypercoordination while the corresponding hydrides were unstable or hard to isolate for detailed structural investigations.[7]

Recently, we demonstrated both experimentally and theoretically that a bare gold atom (without the support of the phosphine ligand) can also behave like a hydrogen atom in silicon−gold compounds.[8] In a systematic study, we showed that $SiAu_2$, $SiAu_3$, and $SiAu_4$ have similar electronic and geometrical structures to the corresponding silicon hydrides. In particular, the tetraauride $SiAu_4$ was observed to be an extremely chemically stable molecule with a very large HOMO-LUMO gap, analogous to the stable SiH_4 molecule. Comparisons of the nature of the charge distribution, the relevant molecular orbitals, and the Si−Au bond energies all suggest that gold, similar to hydrogen, forms highly covalent and directional bonds with silicon.[8]

In the present work, we want to test the generality of the Au/H analogy in larger Si−Au clusters. We produced disilicon−Au clusters, $Si_2Au_n^-$ ($n = 2$ and 4), and investigated their electronic structure and chemical bonding using anion photoelectron spectroscopy (PES) and ab initio calculations. The negative ion technique affords convenient size selectivity and PES is ideal to provide unique electronic information about the neutral species. We have found that combining PES and high-level ab initio calculations offers a particularly powerful approach to investigate the structure and bonding of novel clusters because PES provides essentially an electronic finger-

* To whom correspondence should be addressed at the Pacific Northwest National Laboratory. E-mail: ls.wang@pnl.gov.

10.1021/jp0512560 CCC: $30.25
Published on Web 04/21/2005

print, which can be used to understand the geometrical structures and chemical bonding of the underlying clusters.[9]

It is now well-known that the acetylene and ethylene analogues of silicon do not possess the classical configurations. Instead, they prefer to form hydrogen-bridged or other distorted nonclassical structures.[10] In this study, we demonstrate that the disilicon aurides Si_2Au_2 and Si_2Au_4 also prefer nonclassical structures in exact analogy to the corresponding hydrides. Similar to Si_2H_2, the most stable structure for Si_2Au_2 has a dibridged configuration. For Si_2Au_4 the most stable isomer corresponds to a monobridged structure. More interestingly, we found that the potential energy surfaces of the disilicon−gold systems studied here are also very similar to those of the corresponding hydrides. This study further consolidates the isolobal analogy between a bare gold atom and hydrogen initially discovered in the monosilicon aurides.[8]

Experimental Section

Experimental Method. The experiment was performed with a magnetic-bottle time-of-flight PES apparatus equipped with a laser vaporization cluster source. Details of the experiment have been described previously.[11] Briefly, the second harmonic output of a Q-switched Nd:YAG laser, typically at 10 mJ/pulse and 10 Hz repetition rate, was focused down to a 1 mm spot onto an Au/Si disk target. A helium carrier gas pulse (10 atm backing pressure) was delivered to the laser vaporization nozzle to cool the laser-induced plasma and facilitate cluster formation. Clusters from the source were entrained in the helium carrier gas and underwent a supersonic expansion, which was collimated with a skimmer downstream. Negatively charged clusters were extracted from the collimated cluster beam perpendicularly and were analyzed by a time-of-flight mass spectrometer. The cluster anions of interest were mass-selected before photodetachment by one of the three laser beams: 355 (3.496 eV), 266 (4.661 eV), and 193 nm (6.424 eV). Photoelectron spectra were measured by using the magnetic-bottle time-of-flight photoelectron analyzer with an electron kinetic energy resolution of $\Delta E_k/E_k \sim 2.5\%$. The spectrometer was calibrated with the known spectrum of Au^- and Rh^-.

Theoretical Methods. Both density functional theory (DFT) and molecular orbital (MO) theory were used in the current study. We used the Stuttgart quasirelativistic pseudopotentials and basis sets[12] augmented with two f-type polarization functions (0.498 and 1.461) for gold[13] and the aug-cc-pVTZ basis set for silicon.[14] All the calculations were spin-restricted for closed-shell molecules and spin-unrestricted for open-shell species. All calculations were done under appropriate symmetry constraints. Harmonic frequencies at the B3-LYP level were calculated by using analytical second derivatives to examine the nature of the stationary points. We tested a variety of hybrid and pure density functionals. From previous experience on silicon−gold systems[8] and for the current study, we found the B3-LYP functional[15] gives the best results. Therefore, all the DFT data reported here correspond to the B3-LYP calculations. Vertical detachment energies (VDEs) were calculated by using the generalized Koopman's theorem[16] by adding a correction term to the eigenvalues of the anions. The correction term was estimated by eq 1:

$$\delta E = E_1 - E_2 - \epsilon_{\mathrm{HOMO}} \quad (1)$$

where E_1 and E_2 are the total energies of the anion and neutral in their ground states at the anion equilibrium geometry and ϵ_{HOMO} corresponds to the eigenvalue of the highest occupied molecular orbital of the anion. All DFT calculations were carried out with Gaussian 03.[17]

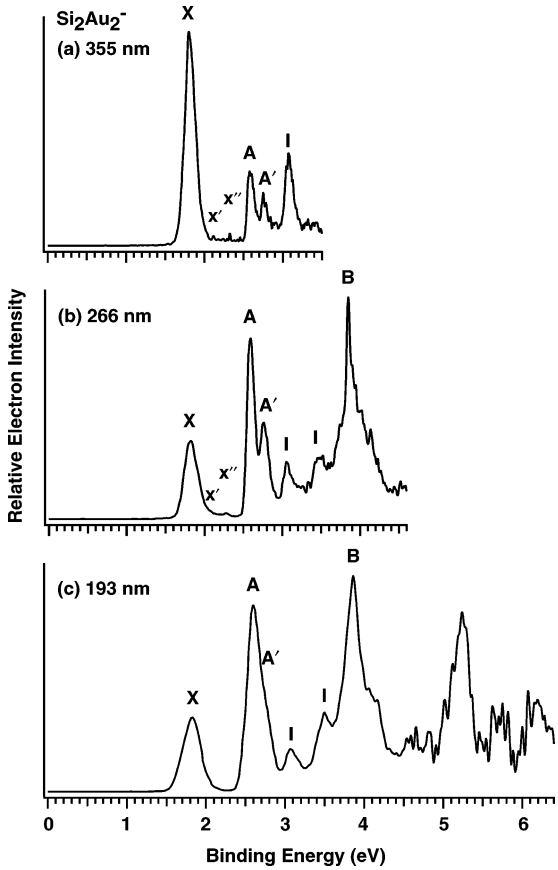

Figure 1. Photoelectron spectra of $Si_2Au_2^-$ at (a) 355 (3.496 eV), (b) 266 (4.661 eV), and (c) 193 nm (6.424 eV). See text for the labels.

To validate the DFT results, we also did a set of calculations using the coupled clusters [CCSD(T)] method.[18] Our coupled-cluster calculations were focused on the lowest energy isomers of $Si_2Au_2^-$ and Si_2Au_2. Full geometry optimizations with the same basis set and pseudopotentials as used in the DFT calculations were employed at the CCSD(T) level. The calculations were done starting from restricted Hatree−Fock wave functions for both the open- and closed-shell molecules. The closed-shell calculations were done with the RCCSD(T) approach and the open-shell calculations were done with the UCCSD(T) approach. All the coupled-cluster calculations were carried out with the MOLPRO package.[19] It was found that the geometries, relative energies, and electron affinities at the B3-LYP level are in excellent agreement with those at the CCSD-(T) level. In general we observed that the B3-LYP relative energies are off by ~0.1−0.2 eV from the corresponding CCSD-(T) values. While the Si−Si and Si−Au bond lengths from these methods were quite close, B3-LYP underestimates the non-bonding Au···Au distances as anticipated. However, when comparisons were made with the experimental results B3-LYP performs quite satisfactorily. Therefore, for the larger systems, $Si_2Au_4^-$ and Si_2Au_4, we used exclusively the B3-LYP method.

Experimental Results

Figures 1 and 2 display the photoelectron spectra of $Si_2Au_n^-$ ($n = 2$ and 4), respectively, at three different photon energies (355, 266, and 193 nm). Numerous transitions were observed in the spectra of the two species. The lowest energy features (X) in the higher resolution 355-nm spectra of both species do not show any trends toward sharpness relative to the 266-nm

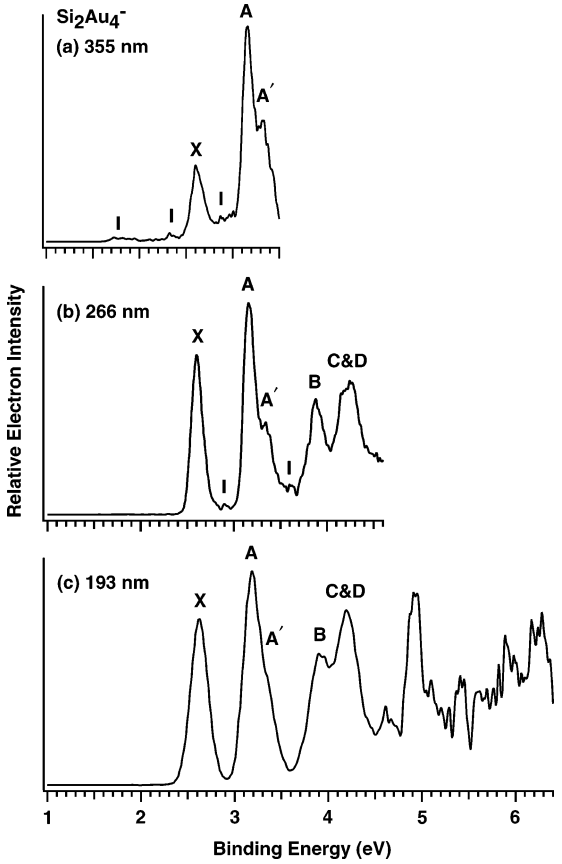

Figure 2. Photoelectron spectra of $Si_2Au_4^-$ at (a) 355 (3.496 eV), (b) 266 (4.661 eV), and (c) 193 nm (6.424 eV). See text for the labels.

spectra. The intrinsic broad width of the X band in both spectra suggests that there is likely a large geometry change between the anions and the neutrals of the two Si−Au clusters. The adiabatic detachment energy (ADE) of the ground-state transition (X), which also represents the electron affinity (EA) of the corresponding neutral cluster, was more difficult to measure without vibrational resolution in the current cases. We estimated the ADE by drawing a straight line at the leading edge of the ground-state feature and then adding a constant to the intersections with the binding energy axis to account for the instrumental resolution. Although this is an approximate procedure, we were able to obtain consistent ADEs from spectra taken at different photon energies. However, if there are extremely large geometry changes between the anion and neutral ground states, the Franck−Condon factor for the 0−0 transition may be negligible, as was observed in our previous work for $SiAu_3^-$ and $SiAu_3$.[8] In such cases, the measured ADEs are merely the detachment thresholds and represent the upper limits for the true ADEs. As we will show in the theoretical section, this is indeed the case for $Si_2Au_2^-$ and $Si_2Au_4^-$ in agreement with the relatively broad width of the X band in Figures 1 and 2.

Both Si_2Au_2 and Si_2Au_4 have even numbers of electrons and may have either singlet (closed shell) or triplet ground states. The PES spectra in Figures 1 and 2 revealed a HOMO-LUMO gap (the X−A separation) for both species: 0.8 eV for Si_2Au_2 and 0.6 eV for Si_2Au_4 (Table 1), which represent the excitation energies of the lowest triplet state in each species. Thus both neutral species should be closed shell systems, as born out in the theoretical calculations (see below). The feature next to the A band, labeled as A′, in both spectra is most likely due to detachment transition to the lowest singlet excited state of the neutral species, judging by their relatively lower intensity compared to that of the A band. The A−A′ separation thus represents the singlet−triplet splitting from detachment of the filled HOMO orbital of the neutral species. The A−A′ separation (~0.17 eV, Table 1) is identical in the spectra of both species. This is a relatively small value, suggesting that the HOMO of Si_2Au_2 and Si_2Au_4 should be primarily Si-based orbitals.

TABLE 1: Experimental Adiabatic (ADE) and Vertical (VDE) Detachment Energies[a] of $Si_2Au_n^-$ (n = 2 and 4)[b]

species	assigned feature	ADE	VDE
$Si_2Au_2^-$	X	1.66(4)	1.79(4)
	x′		2.10(4)
	x″		2.30(4)
	A		2.58(3)
	A′		2.75(3)
	B		3.85(3)
$Si_2Au_4^-$	X	2.46(4)	2.60(3)
	A		3.15(3)
	A′		3.32(3)
	B		3.87(3)
	C		4.18(5)
	D		4.25(5)

[a] All energies are in eV. [b] Numbers in parentheses represent the experimental uncertainty in the last digit.

The PES spectra of $Si_2Au_2^-$ (Figure 1) revealed that the next major peak is around 4 eV labeled as B, with two relatively weak bands (labeled I) between the A and B bands. Except for an intense band around 5.2 eV, the spectral features beyond 4.5 eV had poor signal/noise ratios and were not well defined. Photodetachment from Au 5d-derived molecular orbitals occurs in the higher binding energy region,[9b] consistent with the more congested spectral features. The peaks labeled I in the PES spectra of $Si_2Au_2^-$ were mainly due to contamination of Si_9Au^- as a result of a near mass degeneracy between 7 Si atoms (major isotopmers at mass 196, 197, 198, etc.) and one Au atom (mass 197). The extremely weak features, labeled x′ and x″ in Figure 1 were not related to those features labeled I. These weak features were due to potential minor isomers, as born out in the theoretical results to be shown below.

Beyond band A, the spectra of $Si_2Au_4^-$ (Figure 2) are more complicated with three intense bands around 4 eV (B, C, D). The higher energy part of the $Si_2Au_4^-$ spectra is similar to that of the $Si_2Au_2^-$ spectra. Except for the an intense band at 5.0 eV, this part of the spectra is congested and not very well defined, again likely due to photodetachment from the Au 5d-derived orbitals. The numerous weak signals labeled I in Figure 2 were tentatively assigned to be from contaminations of $Si_9Au_3^-$, similar to the Si_9Au^- contamination in the $Si_2Au_2^-$ spectra (Figure 1). The ADE and VDE for the ground-state transition (X) and the VDEs of the labeled low-lying transitions are given in Table 1 for both species.

Computational Results

Optimized ground-state geometries for $Si_2Au_2^-$ and Si_2Au_2 are shown in Figure 3 and those for $Si_2Au_4^-$ and Si_2Au_4 are displayed in Figures 4 and 5, respectively. Theoretical ADEs and VDEs at B3-LYP and CCSD(T) levels are given in Table 2.

$Si_2Au_2^-$ and Si_2Au_2. Several isomers were considered in the search for the ground-state structures of Si_2Au_2 and $Si_2Au_2^-$ (Figure 3). All the reported isomers for Si_2H_2 were considered.[10c] At both B3-LYP and CCSD(T) levels, the most stable isomer for $Si_2Au_2^-$ is the dibridged structure (**1**). The Si−Si and Si−Au bond lengths and the folding dihedral angles (Au−Si−Si−Au) are 2.30 Å, 2.56 Å, and 124.3°, respectively, at the B3-LYP level and 2.32 Å, 2.50 Å, and 125.3° at CCSD(T) level. The nonbonding Au···Au distance, 4.04 Å at the B3-LYP level

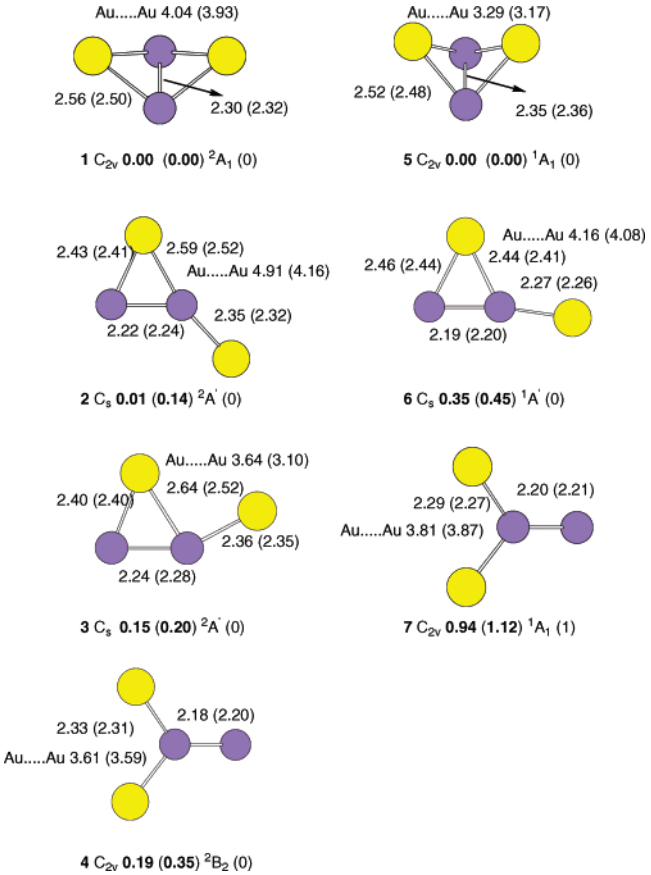

Figure 3. Optimized geometries for $Si_2Au_2^-$ (**1**−**4**) and Si_2Au_2 (**5**−**7**) at B3-LYP and CCSD(T) (in parentheses) levels of theory. Bond lengths are given in Å. The numbers in bold are energies in eV relative to the ground state of the anions for **1**−**4** and for neutrals **5**−**7**.

and 3.93 Å at the CCSD(T) level, indicates weaker aurophilic interaction.[1a] The second isomer, the trans-monobridged structure (**2**), is nearly isoenergetic (0.01 eV) to the ground state at the B3-LYP level. However, the relative energy difference is marginally increased in favor of **1** by 0.14 eV at the CCSD(T) level. The Si−Si bond length in **2** is shortened compared to that in **1** due to the increased π-overlap. Closely following in energy is the cis-monobridged isomer (**3**), which is only 0.15 eV higher in energy than **1** at B3-LYP. While Si−Si and Si−Au bond lengths are quite similar to the trans-isomer, the nonbonding Au····Au distance in the cis-isomer falls within the range of aurophilic interaction.[1a] As expected, the Au···Au distance at the CCSD(T) level (3.10 Å) is much shorter than the corresponding value (3.64 Å) at the B3-LYP level. Consequently, the trans−cis relative energy difference was also reduced: 0.06 eV at the CCSD(T) level compared to 0.14 eV at the B3-LYP level. It should be noted, however, that B3-LYP correctly predicted the relative energy ordering of the isomers and differs quantitatively by 0.1−0.2 eV from the coupled-cluster method. Finally, the auro-disilavinylidene (**4**) with classical bonding features is also a stable isomer higher in energy only by 0.19 eV than the dibridged global minimum at B3-LYP. It is interesting to note that for $Si_2H_2^-$ the relative energy ordering between structures **1** and **4** is exactly in reverse order, i.e., the disilavinylidene is more stable than the dibridged isomer.[20] This indicates that gold has more propensity to form bridges compared to hydrogen.

Unlike $Si_2Au_2^-$, we could locate only two minima (**5** and **6**, Figure 3) on the neutral Si_2Au_2 potential energy surface. Several other isomers were tested and they were either high-order

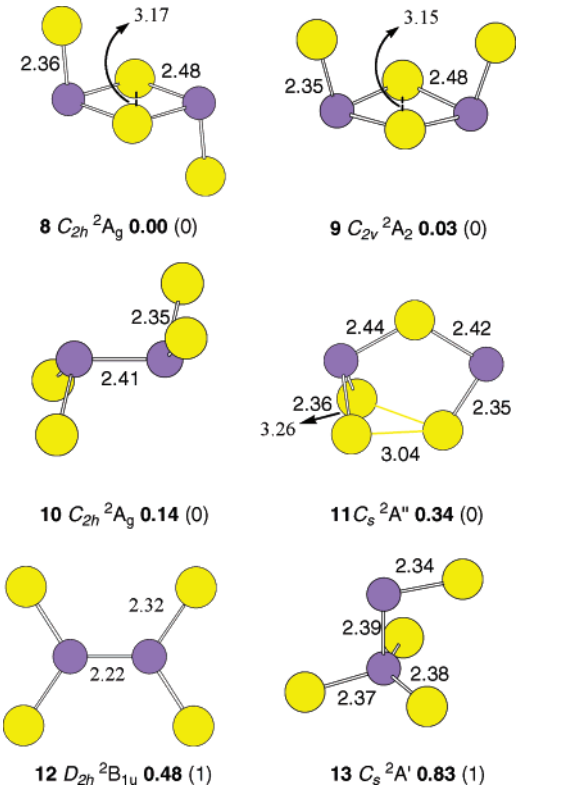

Figure 4. Optimized geometries for $Si_2Au_4^-$ (**8**−**13**) at the B3-LYP level of theory. Bond lengths are given in Å. The numbers in bold are energies in eV relative to the ground state of the anions. The numbers in parentheses are the number of imaginary frequencies.

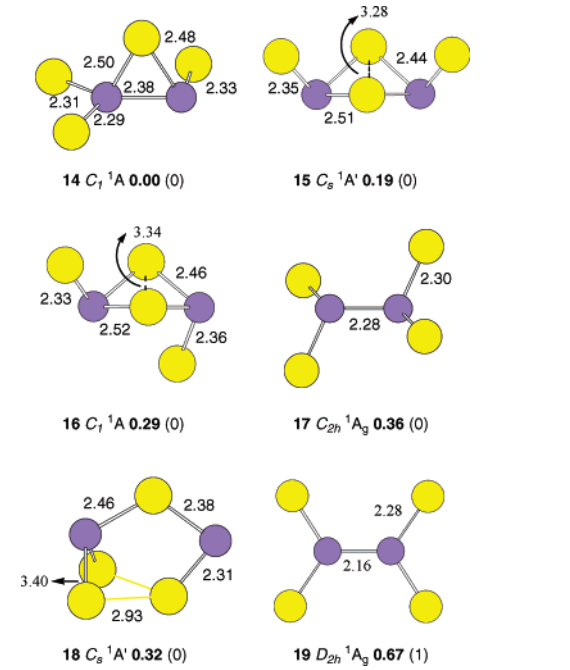

Figure 5. Optimized geometries for Si_2Au_4 (**14**−**19**) at the B3-LYP level of theory. Bond lengths are given in Å. The numbers in bold are energies in eV relative to the ground state of the neutrals. The numbers in parentheses are the number of imaginary frequencies.

stationary points or collapsed to one of the two minima. The dibridged isomer (**5**) is the global minimum for Si_2Au_2, similar to that for the anion $Si_2Au_2^-$, except that the folding angle is significantly reduced in the neutral from 124.3° to 95.4° (at B3-LYP) and from 125.3° to 92.9° [at CCSD(T)]. Similar, but less dramatic, changes in the folding angle have been observed for

TABLE 2: Calculated Detachment Energies (eV) for the Three Isomers of $Si_2Au_2^-$ (1−3) and $Si_2Au_4^-$ (8−10) at B3-LYP

1 (dibridged isomer)				**2** (trans-monobridged isomer)				**3** (cis-monobridged isomer)			
MO[a]	ADE	VDE (singlet)	VDE (triplet)	MO[a]	ADE	VDE (singlet)	VDE (triplet)	MO[a]	ADE	VDE (singlet)	VDE (triplet)
$(14a_1)^{-1}$	1.48 [1.34][b]	1.79 [1.69][b]		$(25a')^{-1}$	1.83 [1.65][b]	2.31 [2.10][b]		$(25a')^{-1}$	1.69 [1.72][b]	2.04 [1.97][a]	
$(13a_1)^{-1}$		2.63	2.54	$(9a'')^{-1}$		2.65	2.57	$(13a'')^{-1}$		2.63	2.55
$(12a_1)^{-1}$		3.85	3.65	$(24a')^{-1}$		3.86	3.56	$(24a')^{-1}$		3.88	3.69
$(8b_1)^{-1}$		5.01	4.88	$(23a')^{-1}$		4.85	4.71	$(23a')^{-1}$		4.79	4.62
$(7b_2)^{-1}$		5.28	5.19	$(22a')^{-1}$		5.56	5.35	$(22a')^{-1}$		5.56	5.39
$(11a_1)^{-1}$		6.03	5.97	$(8a'')^{-1}$		5.81	5.77	$(12a'')^{-1}$		5.75	5.71
$(4a_2)^{-1}$		6.08	6.04	$(21a')^{-1}$		5.81	5.78	$(21a')^{-1}$		5.75	5.71
$(6b_2)^{-1}$		6.16	6.12	$(7a'')^{-1}$		6.23	6.17	$(7a'')^{-1}$		6.10	6.05

8 (*trans*-dibridged isomer)				**9** (*cis*-dibridged isomer)				**10** auro-disilene			
MO[a]	ADE	VDE (singlet)	VDE (triplet)	MO[a]	ADE	VDE (singlet)	VDE (triplet)	MO[a]	ADE	VDE (singlet)	VDE (triplet)
$(9b_g)^{-1}$	2.39	2.62		$(8a_2)^{-1}$	2.26	2.58		$(16a_g)^{-1}$		2.68	
$(18a_g)^{-1}$		3.55	3.49	$(15b_2)^{-1}$		3.72	3.66	$(11b_g)^{-1}$		3.91	3.75
$(17a_g)^{-1}$		4.15	4.12	$(19a_1)^{-1}$		3.76	3.68	$(15b_u)^{-1}$		4.12	3.87
$(16b_u)^{-1}$		4.31	4.23	$(18a_1)^{-1}$		4.49	4.33	$(15a_g)^{-1}$		4.34	4.21
$(10a_u)^{-1}$		4.54	4.32	$(11b_1)^{-1}$		4.56	4.46	$(11a_u)^{-1}$		4.68	4.63
$(15b_u)^{-1}$		5.94	5.81	$(14b_2)^{-1}$		5.91	5.79	$(14b_u)^{-1}$		5.70	5.56
$(9a_u)^{-1}$		5.98	5.97	$(7a_2)^{-1}$		5.96	5.95	$(9b_g)^{-1}$		5.96	5.95
$(16a_g)^{-1}$		6.00	5.99	$(17a_1)^{-1}$		5.99	5.98	$(10a_u)^{-1}$		5.97	5.95
$(8b_g)^{-1}$		6.01	6.00	$(10b_1)^{-1}$		6.00	5.99	$(14b_g)^{-1}$		5.98	5.97

[a] Detachment channel. [b] The numbers in square brackets were calculated at the CCSD(T) level of theory.

the Si_2H_2 systems.[20] Removal of the negative charge enhances folding of the unit and brings gold atoms closer to within the range of significant aurophilic interaction. The only other stable isomer for Si_2Au_2 is the monobridged structure (**6**), which is higher in energy by 0.35 (0.45) eV at B3-LYP [CCSD(T)]. Unlike the anion, there are no cis- and trans-isomers for neutral Si_2Au_2. Upon geometry optimization both structures collapse to the single monobridged structure, in which the $\angle$Si−Si−Au_{edge} angle is nearly linear (171.8° at B3-LYP). The neutral auro-disilavinylidene (**7**) is a transition state with a barrier height of 0.58 (0.67) eV at B3-LYP [CCSD(T)] for the scrambling of the gold atoms from the bridge to the edge position, resulting in the single monobridged isomer, **6**.

$Si_2Au_4^-$ and Si_2Au_4. This stoichiometry corresponds to that of ethylene. However, it is well-known that the corresponding silicon hydride Si_2H_4 does not possess the classical ethylene structure.[10,20−22] Here we found that Si_2Au_4 and its anions also do not assume the conventional structures. These species have much richer potential energy surfaces compared to the carbon analogues. We considered many possible isomers in order to locate the lowest energy structure for $Si_2Au_4^-$, as shown in Figure 4. Most of these structures have direct resemblance to the silicon−hydrogen counterparts.[20,21] However, some of the structures have more "cluster-like" geometries. The most stable isomer is the trans-dibridged structure (**8**) and the cis-isomer (**9**) is almost degenerate with the trans-isomer. These two structures can be constructed by adding two gold atoms to the opposite (trans-) or the same side (cis-) of the most stable isomer of $Si_2Au_2^-$ (**1**) with one major change, that is, there is no Si−Si bonding in **8** and **9**. Instead, the relatively short $Au_{bridge}\cdots Au_{bridge}$ distances, 3.17 Å (**8**) and 3.15 Å (**9**), indicate stronger Au−Au interactions across the four-membered ring.

The trans-bent auro-disilene (**10**), which is the global minimum for Si_2H_4,[21] is only 0.14 eV higher in energy than **8**. The Si−Si bond length (2.41 Å) is close to the single bond length. The two $SiAu_2$ units are nearly perpendicular to the Si−Si bond vector (each $SiAu_2$ unit deviates from planarity with the Si−Si bond vector by 74.2°). The planar, D_{2h} ethylene analogue (**12**) is a transition sate (i151.7 cm^-) with a barrier height of 0.31 eV, connecting the flipping motion of the silicon atoms in disilene to the global minimum (**8**). We have also found an isomer with a cluster-like geometry (**11**), in which three Au atoms seem to cluster on one side of the structure. This structure is 0.34 eV higher in energy than **8** and does not have a Si_2H_4 counterpart. Another important isomer is auro-silylsilylene, **13**. The corresponding silicon hydride, silylsilylene, is higher in energy than disilene by 0.28 eV and is also a minimum.[20] However, our current B3-LYP result suggests that structure **13** lies 0.69 eV above the auro-disilene (**10**) and has one imaginary frequency (i113.2 cm^-) corresponding to the transfer of a gold atom between the two silicon atoms.

For neutral Si_2Au_4 (Figure 5), we found its most stable isomer to be a monobridged structure (**14**) without any symmetry. This is a very interesting structure: except for the bridging atom, the rest of the atoms are nearly planar. The structure can be constructed by rearranging an edge gold atom from the disilene (**19**) to the bridging position. Consequently, the Si−Si bond length increased from 2.16 Å for **19** to 2.38 Å for **14**. There is no anionic state for this structure. Optimization by adding an electron to **14** led to the trans-bent disilene structure (**10**). The neutral counterparts of the cis and trans dibridged structures became low-lying isomers, C_s (**15**) and C_1 (**16**), with reduced symmetries. The neutral trans-bent auro-disilene (**17**) is 0.36 eV above **14**. There is considerable shortening of the Si−Si bond from the anion to neutral [2.41 Å (**10**) and 2.28 Å (**17**)] and the deviation from planarity for the neutral isomer (52.0°) is not as severe as in the case of the anion. The planar auro-disilene (**19**) is 0.67 eV higher in energy than the lowest energy structure and is again a transition state (i190.2 cm^{-1}). Finally, the cluster-like isomer with C_s symmetry (**18**) is 0.32 eV above the ground state with enhanced Au−Au interactions.

Theoretical studies on the potential energy surface of the Si_2H_4 molecule span nearly two decades.[10,20−22] Most of the studies have focused on two isomers: disilene and silylsilylene. All studies agree that disilene is the most stable isomer followed by silylsilylene and the trans- and cis-dibridged structures. Recently, using highly correlated ab initio calculations and the experimental rotational spectrum from microwave spectroscopy,

Sari et al.[21] identified a new monobridged isomer, similar to **14**, which is 0.31 eV above disilene. No such minimum had been observed at SCF.[22] Very expensive but highly desirable CCSD(T) geometry optimizations were needed to locate the C_1 monobridged minimum. We checked the Si_2H_4 structures using B3-LYP with the aug-cc-pVTZ basis set and found that the monobridged isomer is a minimum and is 0.28 eV above disilene. Except for the elongation of one bridged Si−H bond [1.801 Å [CCSD(T)] to 1.829 Å (B3-LYP)], the rest of the geometrical parameters at B3-LYP agree very well with the coupled-clusters calculations. Like the corresponding gold analogue, at B3-LYP there is no anionic state for the monobridged isomer of Si_2H_4; upon optimization the structure collapses to the disilene.

We have shown that the potential energy surface of the gold and hydrogen analogues of the disilicon species are indeed very similar. However, the relative energy differences between the various isomers for $Si_2Au_n^-$ and Si_2Au_n ($n = 2$ and 4) are very closely distributed. Although the dibridged isomers (**1** and **8**) are found to be more stable for the anions of the two Si−Au species, definitive assignments of the global minimum structures become at most tentative considering the limitation and accuracy of the current methods used. Calculations in tandem with experiments are more appropriate for the structural assignments and determination. In the next section, we compare the calculated VDEs of the various anionic isomers with the experimental PES spectra and show that the current calculations provide accurate descriptions of the ground states for the two disilicon auride molecules.

Discussion

$Si_2Au_2^-$. The global minimum of $Si_2Au_2^-$ was predicted to be a doublet (**1**, $^2A_1$, C_{2v}) with a valance configuration of $6b_2^2$-$4a_2^2 11a_1^2 7b_2^2 8b_1^2 12a_1^2 13a_1^2 14a_1^1$. The first electron detachment is from the $14a_1$ MO, which primarily consists of a linear combination of the Si−Si bonding orbital (60%) and the Si−Au−Si 3c−2e (three center-two electron) antibonding orbitals (14% each) (Figure 6a). Detachment of an electron from this MO induces major structural changes. In addition to the marginal increase in Si−Si bond length [2.30 Å (**1**) and 2.35 Å (**5**)] upon detachment, the folding angle decreased substantially in the neutral to allow favorable Au···Au interactions. The calculated VDE for the ground-state transition (detachment from the $14a_1$ orbital) at the B3-LYP level (1.79 eV) is nearly identical with the experimental value (1.79 ± 0.04 eV) (Tables 1 and 2). The VDE for **1** at the CCSD(T) level (1.69 eV) is slightly smaller, but it is also in good agreement with the experiment. The calculated ADE, 1.48 eV (1.34 eV) at the B3-LYP [CCSD(T)] level, however, is far off from the experimental value (1.66 ± 0.04 eV) (Table 1). The large difference between the calculated VDE and ADE (0.31 eV) is due to the large geometry change between the anion and neutral ground state, consistent with the large folding angle change in the dibridged structure (**1**) upon electron detachment (**5**). This result explains the broad width of the X band in Figure 1 and suggests that there is little Franck−Condon factor for the 0−0 transition and the experimentally estimated ADE should be considered only as a threshold value, an upper limit to the true ADE. The lowest VDEs of the trans-isomer (**2**) and cis-isomer (**3**), 2.31 (2.10) and 2.04 (2.06) eV, respectively (Table 2), at B3-LYP [CCSD(T)], do not agree with the ground-state band (X). However, we note that these VDEs are in good agreement with those of the very weak features (x″, 2.30 eV and x′, 2.10 eV) (Table 1), suggesting that these two low-lying isomers were present in the cluster beam, albeit their relative abundances were negligible compared to that of the dibridged global minimum structure (**1**).

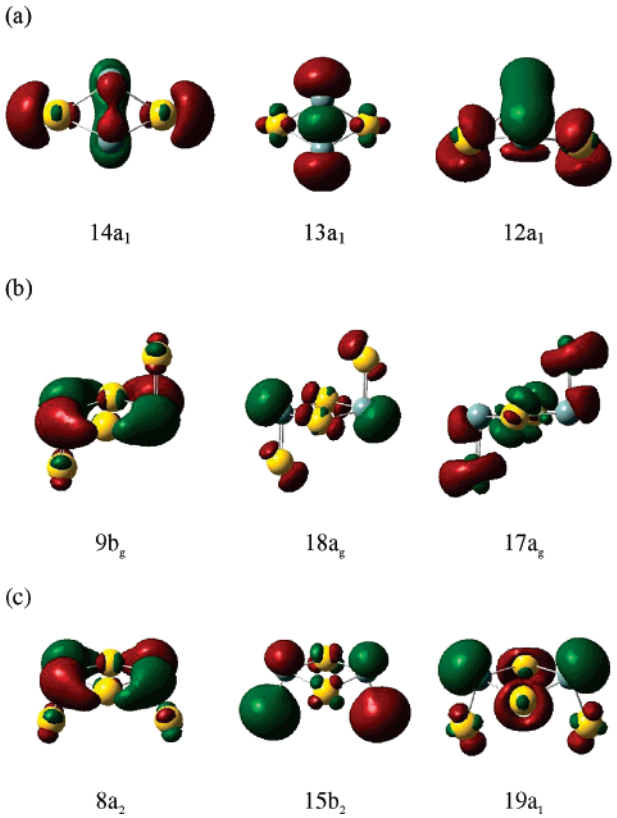

Figure 6. Valence molecular orbital pictures of (a) the dibridged global minimum isomer of $Si_2Au_2^-$ (**1**), (b) the lowest lying trans-dibridged isomer of $Si_2Au_4^-$ (**8**), and (c) the close low-lying cis-dibridged isomer of $Si_2Au_4^-$ (**9**).

The second detachment channel from the global minimum of $Si_2Au_2^-$ is from the $13a_1$ orbital, which is a mixture of Si−Si σ-bond and lone pairs from silicon atoms (Figure 6a). The calculated VDE for the triplet final state (detachment from $13a_1^\beta$) is 2.54 eV, in excellent agreement with the experimental value (2.58 eV) of the A band (Figure 1 and Table 1). The calculated VDE for the singlet final state from $13a_1^\alpha$ is 2.63 eV, in reasonable agreement with the experimental VDE (2.75 eV) of the A′ band (Figure 1 and Table 1). The next detachment channel from the global minimum of $Si_2Au_2^-$ is from the $12a_1$ orbital (Figure 6a). The calculated VDEs for the triplet and singlet final states are 3.65 and 3.85 eV, respectively (Table 2), which are in good agreement with the intense and broad PES spectral feature B centered at 3.85 eV (Figure 1).

The next detachment channel is from the $8b_1$ orbital and higher detachment channels up to 6.4 eV were calculated, as given in Table 2. These higher energy detachment channels are mainly from gold lone pair orbitals (filled d-orbitals). The calculated VDEs from these orbitals are in good agreement with the congested PES spectral pattern above 4.5 eV (Figure 1). The good agreement between the calculated VDEs from the dibridged isomer (**1**) of $Si_2Au_2^-$ and the experimental PES spectra lends considerable credence to the ground state structure obtained theoretically for $Si_2Au_2^-$ (**1**) and Si_2Au_2 (**5**) (Figure 3).

The calculated VDEs for the two low-lying isomers (**2** and **3**) are also given in Table 2. The high binding energy detachment channels of **2** and **3** have a close correspondence to those of the global minimum **1**. However, since their first

detachment channels, which were clearly identified from the PES spectra (x″ and x′, respectively, in Figure 1 and Tables 1 and 2), had negligible intensities in the PES spectra (Figure 1), we suspected that these two isomers would not make much contribution to the high binding energy part of the PES spectra of $Si_2Au_2^-$ shown in Figure 1.

$Si_2Au_4^-$. There are at least two isomers competing for the ground state of $Si_2Au_4^-$: the dibridged trans-isomer (**8**) and cis-isomer (**9**) are nearly isoenergetic. The trans-dibridged isomer with a ^2B_g (C_{2h}) state and $8b_g^2 16a_g^2 9a_u^2 15b_u^2 10a_u^2 16b_u^2 17a_g^2 18a_g^2 9b_g^1$ valence electronic configuration is only 0.03 eV lower than the $^2A_2$ (C_{2v}) cis-isomer with a $10b_1^2 17a_1^2 7a_2^2 14b_2^2 11b_1^2 18a_1^2 19a_1^2 15b_2^2 8a_2^1$ valence electronic configuration. The basic bonding features in these two isomers are very similar except for the orientation of the two terminal gold atoms. The calculated VDEs 2.62 (**8**, from $9b_g^\alpha$) and 2.58 eV (**9**, $8a_2^\alpha$) are both in excellent agreement with the observed value 2.60 eV (Table 1). This detachment channel, which is similar for both the isomers (**8** and **9**), removes an electron from a 3c−2e antibonding orbital consisting of the in-plane silicon p orbitals with marginal coefficients also from the bridge gold atoms (Figure 6b,c). As a result, in the neutral the four-membered ring (Si−Au−Si−Au) distorts substantially from planarity. This is true for both the trans- and cis-isomers. Further enhanced by Au···Au interactions in the neutral both isomers have reduced symmetries (**15** and **16**) with puckered Si−Au−Si−Au rings. This large geometry change is reflected in the calculated ADEs, 2.39 eV for **8** and 2.26 eV for **9** (Table 2), which are significantly smaller than the corresponding VDEs. This result is consistent with the broad width of the X band observed in the PES spectra of $Si_2Au_4^-$ (Figure 2). Similar to the $Si_2Au_2^-$ case, again our measured ADE for $Si_2Au_4^-$ (2.46 eV, Table 1) should be viewed as a upper limit for the true ADE due to the large geometry changes between the anion and neutral states, i.e., the negligible Franck−Condon factors for the 0−0 transition.

The second detachment channel for **8** is from the $18a_g$ orbital, which is primarily a silicon lone pair orbital (Figure 6b). The calculated VDEs for the triplet and singlet final states form this MO are 3.49 and 3.55 eV, respectively (Table 2), which should correspond to the A and A′ bands in the PES spectra of $Si_2Au_4^-$ (Figure 2). However, we noted that the calculated VDEs are significantly higher than the corresponding experimental values (Table 1). The second detachment channel for **9** is from the $15b_2$ orbital, which has major contributions from the Au 6s and silicon lone pairs (Figure 6c). The calculated VDEs for the triplet and singlet final states for this detachment channel are 3.66 and 3.72 eV (Table 2), which are even higher than those from isomer **8** and are in worse agreement with the experimental values than those from isomer **8**. This discrepancy between the calculated and experimental VDEs is probably not surprising considering the size and complexity of the systems and the accuracy of the theoretical method used (B3-LYP).

Higher binding energy detachment channels up to 6 eV were calculated for both **8** and **9** and are given in Table 2. The numbers for the two isomers are similar and they are in general in good agreement with the PES spectra of $Si_2Au_4^-$ (Figure 2). We also computed the VDEs for the auro-disilene isomer (**10**), as also given in Table 2. The calculated VDEs from this isomer clearly disagree with the PES patterns of $Si_2Au_4^-$ and we can rule out any significant contribution of this isomer to the observed PES spectra. However, from both the energetics and the calculated PES spectra, we cannot rule out isomer **9** and conclude that both isomer **8** and **9** may exist in our cluster beam.

SCHEME 1: Valance Bond Description of Si_2Au_2 (5)

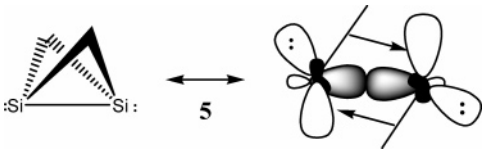

Ultimate determination of which one (**8** or **9**) is the true global minimum for $Si_2Au_4^-$ may require more accurate calculations, which we cannot afford currently. However, the most stable neutral Si_2Au_4 is **14** (Figure 5). Since a similar isomer does not exist in the anion, this neutral structure cannot be accessed experimentally in the current anion PES study.

The Chemical Bonding in Si_2Au_2 and Si_2Au_4 and Comparisons to That in Si_2H_2 and Si_2H_4

In our prior work on $SiAu_n$ ($n = 2-4$),[8] we discovered the H analogy of a single Au atom and established firmly the similarity in the chemical bonding between the silicon auride and the corresponding silicon hydrides (SiH_n) from both MO analyses and bond energy considerations. In the present work, we found similar analogies between the disilicon aurides and their corresponding hydrides and reinforce the concept that Au may behave like H in forming novel auride molecules.

The nonclassical bonding in different structural isomers of Si_2H_2, Si_2H_4, and the corresponding heavier group IV hydrides is now well established. There are essentially two bonding models.[23] In the Carter, Goddard, Malrieu, and Trinquier model (CGMT),[24] the distortion from the classical bonding was explained in terms of the ground-state properties of Si−H and SiH_2. In this model, the factors that determine the nonplanar trans-bent form are the singlet−triplet excitation energy of the fragment SiH_2 ($\Delta E_{(S-T)}$) and the Si═Si double bond energy ($E_{\sigma-\pi}$). If $\sum\Delta E_{(S-T)} < {}^1/_2 E_{\sigma-\pi}$, then the classical bonding is observed; otherwise trans-bent forms are preferred. In the molecular orbital model,[25] the trans-bending is explained by the mixing of σ^* and π orbitals. As one moves down the periodic table, the s and p orbitals become more diffuse with the increase in the size of the atomic number. As a result, the σ^* orbitals are lowered in energy and the π orbitals are pushed up. Thus the gap between the π and σ^* becomes small, making it possible for them to mix. This mixing transforms the π bond to a lone-pair-like orbital. In other words, the nonplanar distortion is a result of the second-order Jahn−Teller effect. In either model it is essential to understand the nature of the fragments involved. Before attempting to describe the bonding in Si_2Au_2 and Si_2Au_4, we first compare the $SiAu_2$ and SiAu fragments with the corresponding hydrogen analogues.

SiH_2 has a singlet ground state. The singlet−triplet (S−T) energy gap at the B3-LYP/aug-cc-pVTZ level is 0.89 eV. In our earlier paper, we have shown that $SiAu_2$ also has a singlet ground state,[8] with a calculated S−T gap of 1.10 eV. Similarly, the doublet−quartet splitting for Si−H and Si−Au is 1.89 and 1.67 eV, respectively, from our B3-LYP calculations. Unlike the high electronegative substitution, gold is neither excessively stabilizing nor destabilizing relative to the respective electronic states of the silicon hydrogen systems. This indicates that the molecules derived from these fragments should have similar structural features. This indeed was what we observed, as shown in Figures 3−5.

Bonding in the Si_2Au_2 dibridged structure (**5**) is quite similar to that of the corresponding hydrogen system. Basically there are one Si−Si σ-bond, two 3c−2e (Si−Au−Si) bonds, and two lone pairs on each of the silicon atoms (Scheme 1). This simple

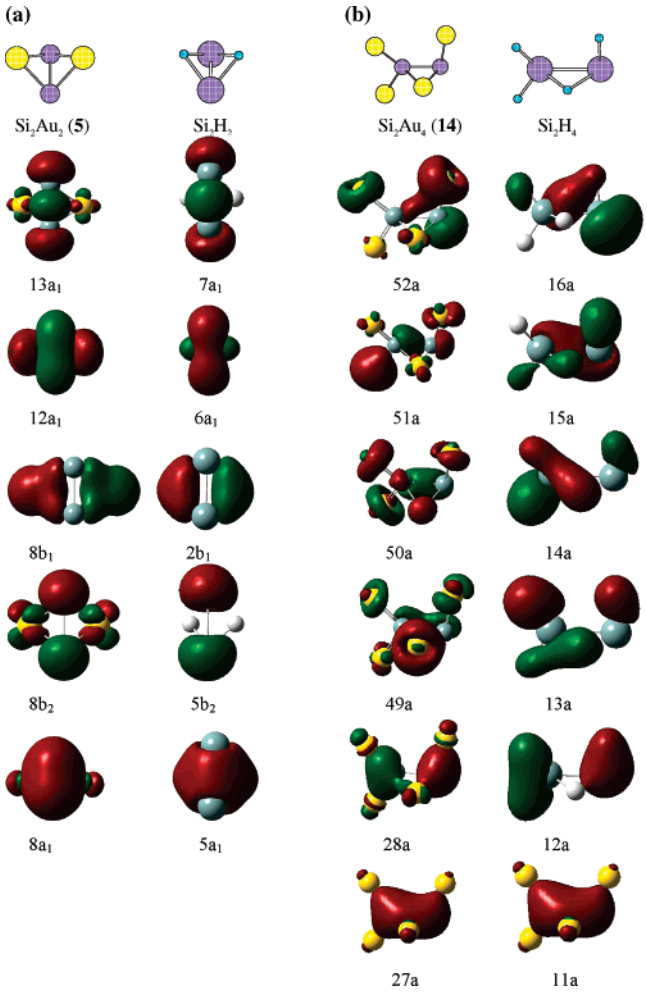

Figure 7. (a) Comparisons of the five bonding molecular orbitals of the global minimum dibridged structure of Si_2Au_2 (**5**) with the corresponding structure and molecular orbitals of Si_2H_2. (b) Comparison of the six bonding molecular orbital pictures of the global minimum monobridged structure of Si_2Au_4 (**14**) and the corresponding structure and molecular orbitals of Si_2H_4.

valance bond picture captures the essential bonding features in **5**. All five bonding MOs for both Si_2H_2 and Si_2Au_2 are given and compared in Figure 7a. The HOMO of both systems is a linear combination of Si−Si σ-bond and silicon lone pair orbitals. Both HOMO-1 and HOMO-2 are the 3c−2e bonds involving Si−Au(H)−Si units. The remaining two orbitals are clearly a silicon lone pair ($8b_2/5b_2$) and an all bonding orbital ($8a_1/5a_1$). Thus, there is a one-to-one correspondence between the Si_2H_2 and Si_2Au_2 systems in both their structure and bonding.

The ground state of Si_2Au_4 is the monobridged isomer **14** (Figure 5). This unusual bridged isomer was first reported by Trinquier in 1991 for Sn_2H_4 and Pb_2H_4.[22] Using SCF/DZP and CASCF+OVB methods, Trinquier observed that this unsymmetrical arrangement was a minimum for Sn and Pb but not a minimum for Si and Ge. Trinquier further noticed that these singly bridged isomers can be topologically connected to the other isomers, e.g., the dibridged trans- and cis-isomers, and the trans-bent double-bonded form. Combining microwave spectroscopic experiments and highly correlated couple-cluster calculations, Sari et al.[21] recently identified that Si_2H_4 also has a monobridged minima similar to Sn and Pb. Our own calculation at the B3-LYP/aug-cc-pVTZ level also located the monobridged minimum for Si_2H_4. The bonding in Sn_2H_4 and Pb_2H_4 had been analyzed as two singlet XH_2 moieties bound by a 3c−2e bridge and an $n_\sigma \rightarrow p_\pi$ dative bond.[22]

SCHEME 2: Valance Bond Description of Si_2Au_4 (14 and 17)

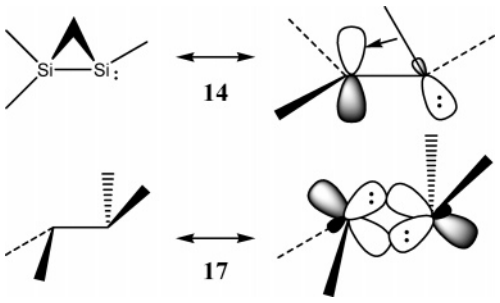

The six bonding MOs for the global minimum monobridged Si_2Au_4 (**14**) are compared to those of the monobridged Si_2H_4 in Figure 7b. In a simple valance bond pictorial representation and according to the natural bond orbital analysis, the bonding in this isomer can be represented as a Si−Si σ-bond and Si−Au(H)−Si 3c−2e bond with three Si−Au(H) σ-bonds and a lone pair on one of the silicon atoms (Scheme 2). By virtue of the lack of symmetry the corresponding canonical MOs (CMO) are heavily mixed. From our CMO analysis, the HOMO (52a in Figure 7b) is an out-of-phase mixture of the Si−Au bond (30%) and the Si lone pair (25%) with some mixing from another Si−Au bond and the Si−Si bond. Other bonding orbitals are also highly mixed, but the similarity between the MOs of Si_2Au_4 and Si_2H_4 in Figure 7b is clearly revealed. Analogously, we have also analyzed the bonding and MOs in the trans (**16**) and cis (**15**) dibridged isomers and the trans-bent double bonded system (**17**) and found that they are also identical with the corresponding Si_2H_4 systems. A valence bond picture describing the bonding in the trans-bent auro-disilene (**17**) is also shown in Scheme 2.

Conclusions

A combined photoelectron spectroscopic and theoretical study was carried out on the $Si_2Au_2^-$ and $Si_2Au_4^-$ systems. Well-resolved PES spectral features were obtained and compared to the theoretical calculations. Extensive electronic structure calculations at the density functional theory and CCSD(T) level were performed to elucidate the ground-state structures of $Si_2Au_2^-$ and $Si_2Au_4^-$ and their neutral species. The B3-LYP functional with the properly chosen basis set yielded results competitive with those by CCSD(T). In both anion and neutral of the Si_2Au_2 systems a dibridged structure was found to be the ground state. For $Si_2Au_4^-$, trans and cis dibridged isomers were found to be the lowest energy isomers, which are nearly degenerate. However, the most stable structure in the neutral potential energy surface of Si_2Au_4 is the monobridged isomer. The potential energy surface and the nature of bonding in Si_2Au_2 and Si_2Au_4 were found to be similar to those of the corresponding hydrogen analogues. This study further strengthens the isolobal analogy between gold and hydrogen in forming novel Si−Au clusters.

Acknowledgment. This work was supported by the U.S. National Science Foundation (CHE-0349426) and performed at the EMSL, a national scientific user facility sponsored by the U.S. DOE's Office of Biological and Environmental Research and located at the Pacific Northwest National Laboratory, operated for DOE by Battelle. Calculations were performed both with our local PC cluster and on the supercomputers at the EMSL Molecular Science Computing Facility.

References and Notes

(1) For general reviews see: (a) Pyykko, P. *Angew. Chem., Int. Ed.* **2004**, *43*, 4412. (b) Schwarz, H. *Angew. Chem., Int. Ed.* **2003**, *42*, 4442. (c) Schwerdtfeger, P. *Angew. Chem., Int. Ed.* **2003**, *42*, 1892. (d) Schwerdtfeger, P. *Heteroat. Chem.* **2002**, *13*, 578. (e) In *Gold. Progress in Chemistry, Biochemistry and Technology*; Schmidbaur, H., Ed.; Wiley: Chichester, UK, 1999; p 894.

(2) Desclaux, J. P.; Pyykko, P. *Chem. Phys. Lett.* **1976**, *39*, 300.

(3) For reviews on auride chemistry see: (a) Jansen, M.; Murding, A. V. In *Gold. Progress in Chemistry, Biochemistry and Technology*; Schmidbaur, H., Ed.; Wiley: New York, 1999; p 747. (b) Pyykko, P. *Angew. Chem., Int. Ed.* **2002**, *41*, 3573. (c) Gagliardi, L. *J. Am. Chem. Soc.* **2003**, *125*, 7504.

(4) (a) Mingos, D. M. P. *Pure Appl. Chem.* **1980**, *52*, 705. (b) Lauher, J. W.; Wald, K. *J. Am. Chem. Soc.* **1981**, *103*, 7648. (c) Hall, K. P.; Mingos, D. M. P. *Prog. Inorg. Chem.* **1984**, *32*, 237. (d) Burdett, J. K.; Eisensten, O.; Schweizer, W. B. *Inorg. Chem.* **1994**, *33*, 3261.

(5) Kruger, S.; Stener, M.; Mayer, M.; Nortemann, F.; Rosch, N. *J. Mol. Struct.* (*THEOCHEM*) **2000**, *527*, 63.

(6) (a) Scherbaum, F.; Grohmann, A.; Muller, G.; Schmidbaur, H. *Angew. Chem., Int. Ed. Engl.* **1989**, *28*, 463. (b) Grohmann, A.; Schmidbaur, H. *Nature* **1990**, *345*, 140. (c) Schmidbaur, H.; Steigelmann, O. *Z. Naturforsch.* **1992**, *47b*, 1721. (d) Li, J.; Pyykko, P. *Inorg. Chem.* **1993**, *32*, 2630. (d) Schmidbaur, H.; Gabbai, F. P.; Schier, A.; Riede, J. *Organometallics* **1995**, *14*, 4969.

(7) Olah, G. A.; Rasul, G. *Acc. Chem. Res.* **1997**, *30*, 245.

(8) Kiran B.; Li, X.; Zhai, H.-J.; Cui, L. F.; Wang, L. S. *Angew. Chem., Int. Ed.* **2004**, *43*, 2125.

(9) (a) Boldyrev, A.; Wang, L. S. *J. Phys. Chem. A* **2001**, *105*, 10759. (b) Hakkinen, H.; Yoon, B.; Landman, U.; Li, X.; Zhai, H. J.; Wang, L. S. *J. Phys. Chem. A* **2003**, *107*, 6168.

(10) (a) Lischka, H.; Kohler, H. *J. Am. Chem. Soc.* **1983**, *105*, 6646. (b) Bogey, M.; Bolvin, H.; Demuynck, C.; Destombes, J. L. *Phys. Rev. Lett.* **1991**, *66*, 413. (c) Grev, R. S.; Schaefer, H. F. *J. Chem. Phys.* **1992**, *97*, 7990. (d) West, R.; Fink, M. L.; Michl, J. *Science* **1981**, *214*, 1343. (e) Andrews, L.; Wang, X. *J. Phys. Chem. A* **2002**, *106*, 7696.

(11) (a) Wang, L. S.; Cheng, H. S.; Fan, J. *J. Chem. Phys.* **1995**, *102*, 9480. (b) Wang, L. S.; Wu, H. In *Advances in Metal and Semiconductor Clusters. IV. Cluster Materials*; Duncan, M. A., Ed.; JAI: Greenwich, CT, 1998; p 299.

(12) (a) Dolg, M.; Wedig, U.; Stoll, H.; Preuss, H. *J. Chem. Phys.* **1987** *86*, 866. (b) Dolg, M. In *Modern Methods and Algorithms of Quantum Chemistry*; Grotendorst, J., Ed.; NIC Series; Julich Research Center: Julich, Germany, 2000; Vol. 1. (c) Leininger, T.; Berning, A.; Nicklass, A.; Stoll, H.; Werner, H.-J.; Flad, H.-J. *Chem. Phys.* **1997**, 217. (d) Kuchle, W.; Dolg, M.; Stoll, H.; Preuss, H. *Pseudopotentials of the Stuttgart/Dresden Group* **1998** (Revision: Tue Aug 11, 1998). See World Wide Website: http://www.theochem.uni-stuttgart.de/pseudopotentiale).

(13) Martin, J. M. L.; Sundermann, A. *J. Chem. Phys.* **2001**, *114*, 3408.

(14) Kendall, R. A.; Dunning, T. H., Jr.; Harrison, R. J. *J. Chem. Phys.* **1992**, *96*, 6796.

(15) (a) Becke, A. D. *J. Chem. Phys.* **1993**, *98*, 5648. (b) Lee, C.; Yang, W.; Parr, R. G. *Phys. Rev. B* **1988**, *37*, 785. (c) Vosko, S. H.; Wilk, L.; Nusair, M. *Can. J. Phys.* **1980**, *58*, 1200. (d) Stephens, P. J.; Devlin, F. J.; Chabalowski, C. F.; Frish, M. J. *J. Phys. Chem.* **1994**, *98*, 11623.

(16) Tozer, D. J.; Handy, N. C. *J. Chem. Phys.* **1998**, *109*, 10180.

(17) Frisch, M. J.; et al. *Gaussian 03*, rev. B. 04; Gaussian, Inc.: Pittsburgh, PA, 2003.

(18) Watts, J. D.; Gauss, J.; Bartlett, R. J. *J. Chem. Phys.* **1993**, *98*, 8718.

(19) Werner, H.-J.; Knowles, P. J.; Amos, R. D.; Bernhardsson, A.; Berning, A.; Celani, P.; Cooper, D. L.; Deegan, M. J. O.; Dobbyn, A. J.; Eckert, F.; Hampel, C.; Hetzer, G.; Korona, T.; Lindh, R.; Lloyd, A. W.; McNicholas, S. J.; Manby, F. R.; Meyer, W.; Mura, M. E.; Nicklass, A.; Palmieri, P.; Pitzer, R. M.; Rauhut, G.; Schutz, M.; Stoll, H.; Stone, A. J.; Tarroni, R.; Thorsteinsson, T. MOLPRO-2002, a package of initio programs written at the Universitat Stuttgart, Stuttgart, Germany, and the University of Birmingham, Birmingham, United Kingdom, 2002.

(20) Pak, C.; Rienstara-Kiracofe, J. C.; Schaefer, H. F. *J. Phys. Chem. A* **2000**, *104*, 11232.

(21) Sari, L.; McCarthy, M. C.; Schaefer, H. F.; Thaddeus, P. *J. Am. Chem. Soc.* **2003**, *125*, 11409.

(22) Trinquier, G. *J. Am. Chem. Soc.* **1991**, *113*, 144.

(23) (a) Trinquier, G.; Malrieu, J. P. *J. Phys. Chem.* **1990**, *94*, 6184. (b) Power, P. P. *Chem. Rev.* **1999**, *99*, 3463.

(24) (a) Carter, E. A.; Goddard, W. A., III *J. Phys. Chem.* **1986**, *90*, 998. (b) Trinquier, G.; Malrieu, J. P. *J. Am. Chem. Soc.* **1987**, *109*, 5303. (c) Trinquier, G.; Malrieu, J. P. In *The chemistry of functional groups. Suppl. A: The chemistry of double bonded functional groups*; Patai, S., Ed.; Wiley: Chichester, 1989; Vol. 2, Part I, p 1. (d) Trinquier, G. *J. Am. Chem. Soc.* **1990**, *112*, 2130. (e) Jacobson, H.; Ziegler, T. *J. Am. Chem. Soc.* **1994**, *116*, 3667. (f) Takahashi, M.; Sakamoto, K. *J. Phys. Chem. A* **2004**, *108*, 5710.

(25) (a) Albright, T. A.; Burdett, J. K.; Wangbo, M. H. *Orbital Interactions in Chemistry*; Wiley: New York, 1985; p 166. (b) Driess, M.; Grutzmacher, H. *Angew. Chem., Int. Ed. Engl.* **1996**, *35*, 828. (c) Kutzelnigg, W. *Angew. Chem., Int. Ed. Engl.* **1984**, *23*, 272.